Article

Glucosylceramide Reorganizes Cholesterol-Containing Domains in a Fluid Phospholipid Membrane

Ana R. P. Varela,[1,2,3] André Sá Couto,[1] Aleksander Fedorov,[2] Anthony H. Futerman,[3] Manuel Prieto,[2] and Liana C. Silva[1,*]

[1]iMed.ULisboa-Research Institute for Medicines, Faculdade de Farmácia and [2]Centro de Química-Física Molecular and IN-Institute of Nanoscience and Nanotechnology, Instituto Superior Técnico, Universidade de Lisboa, Lisbon, Portugal; and [3]Department of Biological Chemistry, Weizmann Institute of Science, Rehovot, Israel

ABSTRACT   Glucosylceramide (GlcCer), one of the simplest glycosphingolipids, plays key roles in physiology and pathophysiology. It has been suggested that GlcCer modulates cellular events by forming specialized domains. In this study, we investigated the interplay between GlcCer and cholesterol (Chol), an important lipid involved in the formation of liquid-ordered (l_o) phases. Using fluorescence microscopy and spectroscopy, and dynamic and electrophoretic light scattering, we characterized the interaction between these lipids in different pH environments. A quantitative description of the phase behavior of the ternary unsaturated phospholipid/Chol/GlcCer mixture is presented. The results demonstrate coexistence between l_o and liquid-disordered (l_d) phases. However, the extent of l_o/l_d phase separation is sparse, mainly due to the ability of GlcCer to segregate into tightly packed gel domains. As a result, the phase diagram of these mixtures is characterized by an extensive three-phase coexistence region of fluid (l_d-phospholipid enriched)/l_o (Chol enriched)/gel (GlcCer enriched). Moreover, the results show that upon acidification, GlcCer solubility in the l_o phase is increased, leading to a larger l_o/l_d coexistence region. Quantitative analyses allowed us to determine the differences in the composition of the phases at neutral and acidic pH. These results predict the impact of GlcCer on domain formation and membrane organization in complex biological membranes, and provide a background for unraveling the relationship between the biophysical properties of GlcCer and its biological action.

INTRODUCTION

Membrane lipids play an active role in diverse cellular events, including cell growth, differentiation, and migration (1,2). Sphingolipids (SLs) are an important lipid class and include a number of bioactive lipid species, ranging from sphingoid backbones to more complex glycosphingolipids (GSLs) (3). Even though the existence of lipid domains is still highly controversial, several studies have linked the bioactive roles of SLs to their ability to form specialized domains that, due to their distinct lipid and protein compositions, display different biophysical properties. The most common examples are lipid raft domains (4) and ceramide platforms (5). Whereas ceramide platforms display properties typical of the gel phase (6,7), lipid raft domains are described as l_o regions—an intermediate state between the gel (or solid ordered, s_o) and fluid (liquid-disordered, l_d) phases. Accordingly, the lipids in the l_o phase have a high degree of conformational order of the acyl chains, similarly to the gel phase, but a fast translational mobility, as in the fluid phase (8). Favorable interactions between SLs and cholesterol (Chol) are one of the underlying principles of lipid rafts (4).

GSLs are an important subgroup of SLs that have also been implicated in membrane domain formation (9,10). Structurally, these lipids consist of a ceramide backbone linked via an ester bond to one or more sugar residues. GSLs are normally found in the outer leaflet of the plasma membrane, where they exert some of their biological roles (e.g., cell-cell communication) and act as receptors for pathogens (11). Glucosylceramide (GlcCer), one of the simplest GSLs, is present in different concentrations in mammalian tissues, reaching up to 95.34 ± 1.77 pmol/mg (~0.0069% of total lipids) in mouse spleen (12). In comparison to other important membrane lipids, GlcCer levels are quite low. For example, it was reported that Cer levels in the spleen are normally ~148.08 ± 14.01 pmol/mg (~0.0082% of total lipids) (12), whereas SM levels vary from 2% to 15% of the total lipids depending on the analyzed tissue (13). GlcCer is an important regulator of a number of cellular events, including calcium homeostasis (14) and endocytic trafficking (15). Although much evidence links the physiological roles of this lipid to its biophysical properties, only a few studies have addressed the impact of GlcCer on membrane properties. We and others have previously reported that GlcCer causes significant changes in the biophysical properties of fluid model membranes, such as an increase in membrane order and the formation of highly ordered gel domains (16–19). These alterations are related to the high melting temperature (T_m) of this lipid (20), its small

uncharged headgroup, and its ability to function as both a donor and an acceptor for hydrogen (H)-bond formation, which together contribute to its low miscibility in fluid phases and segregation into domains with a high packing density (17,18). Moreover, GlcCer promotes strong morphological alterations in vesicles, driving tubular structure formation (16). These structural alterations are enhanced upon acidification of the membrane environment, even though the ability of GlcCer to form tightly packed gel domains is decreased (21). However, little is known about the effect of this lipid on more complex membrane mixtures. Studies performed in membranes containing Chol or Chol/sphingomyelin (SM) suggested that GlcCer has a low tendency to associate with sterol-enriched domains (18,22). However, similar to what has been described for ceramide (23), this interplay may depend on the content of each lipid. To further elucidate this issue, we performed a thorough study that provides a framework for understanding the interplay between GlcCer and Chol under different conditions. We investigated these interactions using mixtures composed of different GlcCer/Chol molar ratios in a fluid phospholipid matrix. We characterized the biophysical properties and phase behavior of ternary 1-palmitoyl-2-oleoyl-*sn*-glycero-3-phosphocholine (POPC)/Chol/GlcCer mixtures using an array of biophysical methodologies. Partial ternary phase diagrams were determined to quantitatively describe the phase behavior of these mixtures. The results show that even though GlcCer displays a strong tendency to separate into GlcCer-enriched gel domains, it is also able to interact with Chol and form domains displaying l_o properties. These interactions are more favorable at acidic pH, likely due to the decreased ability of GlcCer to form gel domains (21).

MATERIALS AND METHODS

Materials

POPC, D-glucosyl-β-1,1'N-palmitoyl-D-*erythro*-sphingosine (C16-GlcCer), N-rhodamine-dipalmitoylphosphatidylethanolamine (Rho-DOPE), and 1,2-dioleoyl-*sn*-glycero-3-phosphoethanolamine-*N*-(cap biotinyl) (DOPE-biotin) were obtained from Avanti Polar Lipids (Alabaster, AL). *Trans*-parinaric acid (t-PnA) and 1,2-dipalmitoyl-*sn*-glycero-3-phosphoethanolamine-N-(7-nitro-2-1,3-benzoxa-diazol-4yl) (NBD-DPPE) were obtained from Molecular Probes (Leiden, The Netherlands). Chol was obtained from Sigma-Aldrich (St. Louis, MO). All organic solvents were UVASOL grade and obtained from Merck (Darmstadt, Germany).

Methods

Liposome preparation

Multilamellar vesicles (MLVs) and large unilamellar vesicles (LUVs) (total lipid concentration of 0.1 mM) containing lipids and probes were prepared as previously described (24). The suspension medium used was PBS (10 mM sodium phosphate, 150 mM sodium chloride, and 0.1 mM EDTA, pH 7.4) or citrate-phosphate buffer (100 mM citric acid and 200 mM sodium phosphate, pH 5.5). The concentrations of the C16-GlcCer

and Chol stock solutions were determined gravimetrically with a high-precision balance (Metler Toledo UMT2, Greifensee, Switzerland), and the concentration of the POPC stock solution was determined by phosphorus analysis (25). The concentration of the stock solutions of the probes was determined spectrophotometrically using ε (t-PnA, 299.4 nm, ethanol) $= 89 \times 10$ M^{-1}cm^{-1} (26), ε (NBD, 458 nm, chloroform) $= 21 \times 10^3$ M^{-1}cm^{-1} (27), and ε (Rho-DOPE, 559 nm, chloroform) $= 95 \times 10^3$ M^{-1}cm^{-1} (27).

Fluorescence spectroscopy

The fluorescence anisotropy of t-PnA was measured in an SLM Aminco 8100 series 2 spectrofluorimeter with double excitation and emission monochromators (MC-400; Spectronics, Rochester, NY). All measurements were performed at room temperature in 0.5 cm × 0.5 cm quartz cuvettes. The t-PnA excitation (λ_{exc})/emission (λ_{em}) wavelengths were 320/405 nm and the probe/lipid ratio used was 1:500. A constant temperature was maintained using a Julabo F25 circulating water bath controlled with 0.1°C precision directly inside the cuvette with a type-K thermocouple (Electrical Electronic, Taipei, Taiwan).

Time-resolved fluorescence measurements with t-PnA were performed by using the single-photon-timing technique with a laser pulse excitation (28) adjusted to $\lambda_{exc} = 305$ nm (using a secondary laser of Rhodamine 6G (29)) and $\lambda_{em} = 405$ nm. The experimental decays were analyzed using TRFA software (Scientific Software Technologies Center, Minsk, Belarus).

Confocal fluorescence microscopy

Giant unilamellar vesicles (GUVs) were prepared by electroformation (30,31) using the appropriate lipids: DOPE-biotin (at a biotinylated/nonbiotinylated lipid ratio of 1:10^6), Rho-DOPE, and NBD-DPPE (at a probe/lipid ratio of 1:500 and 1:200, respectively). The GUVs were then transferred to eight-well Ibidi μ-slides that had been previously coated with avidin (at 0.1 mg/mL) to improve GUV adhesion to the plate (32). PBS or citrate-phosphate was then added to create a neutral (7.4) or acidic (5.5) environment, respectively. Confocal fluorescence microscopy was performed using a Leica TCS SP5 inverted microscope (DMI6000; Leica Mycrosystems CMS, Mannheim, Germany) with a 63× water (1.2 numerical aperture) apochromatic objective. NBD-DPPE and Rho-DOPE excitation was performed using the 458 nm and 514 nm lines, respectively, from an Ar$^+$ laser. The emission was collected at 480–530 and 530–650 nm for NBD-DPPE and Rho-DOPE, respectively. Confocal sections <0.4 μm thick were obtained using a galvanometric motor stage. Three-dimensional (3D) projections were obtained using Leica Application Suite-Advanced Fluorescence software.

Dynamic light-scattering measurements

The mean diameter and polydispersity index (PdI) of the vesicles were determined by dynamic light-scattering (DLS) analysis on a Zetasizer Nano S (Malvern Instruments, UK). Size measurements were made using the patented noninvasive backscatter (NIBS) technology. Samples were placed in 12-mm-square polystyrene cuvettes and then in a chamber maintained at 25°C. Data were analyzed using the accompanying software (Zetasizer Software 7.03) and expressed as an average size or as a size distribution by intensity. The PdI for each sample was also calculated using the same software. In each experiment, measurements were performed in triplicate.

Electrophoretic light-scattering measurements (ζ-potential determination)

The ζ potential (ZP) was determined by electrophoretic mobility on a ZetaSizer Nano Z system (Malvern Instruments, UK) using the M3-PALS technology. Samples were placed in clear, disposable ζ cells and then in a chamber maintained at 25°C. Data were analyzed using the accompanying software (Zetasizer Software 7.03). In each experiment, measurements were performed in triplicate.

RESULTS

POPC/Chol mixtures

We first characterized the effect of pH on the biophysical and surface charge properties of binary POPC/Chol mixtures. Increasing the Chol content of the mixtures led to an increase in the fluorescence anisotropy of t-PnA (Fig. 1 A), consistent with the formation of a Chol-enriched l_o phase (29). This is further supported by the increase in the mean fluorescence lifetime (Fig. 1 B) and long-lifetime component of t-PnA fluorescence intensity decay toward values typical of a l_o-phase (Fig. 1 C). Both the fluorescence anisotropy and lifetime of t-PnA were higher at pH 7.4 (Fig. 1, A–C), suggesting that there is a global decrease in the order of the membrane upon acidification.

Further characterization using DLS revealed that only a slight increase in the average size of the vesicles, from ~125 to ~140 nm, is observed with increasing Chol content (Fig. S1 A in the Supporting Material). Similar, albeit slightly higher, values were obtained under acidic conditions. This was further confirmed by an analysis of scattering intensities and PdI (Fig. S1, B–D). Mixtures containing 40 mol % Chol were the exception, inasmuch as they displayed a tendency to aggregate and/or fuse, as demonstrated by the high scattered light intensities recorded in the range of 3.5–6.5 μm (Fig. S1, B and C). However, this corresponded to only a small percentage of aggregated vesicles (data not shown). Analysis of the ZP of the vesicles showed that at neutral pH, a significant decrease in the net surface charge of the vesicles occurred after addition of Chol in the mixtures (Fig. S1 E). In contrast, no variation was observed upon acidification of the mixtures (Fig. S1 E).

We further characterized the POPC/Chol mixtures by confocal microscopy, using NBD-DPPE and Rho-DOPE as probes for different lipid phases (Fig. S2). NBD-DPPE has a similar partition between the l_d and l_o phases (33), whereas Rho-DOPE is a probe that is typically excluded from l_o phases (30). NBD-DPPE and Rho-DOPE uniformly labeled the POPC/Chol vesicles, suggesting that no l_d/l_o phase separation occurs in POPC/Chol mixtures (Fig. S2). We previously discussed the difficulty of identifying a POPC/Chol-enriched l_o domain (29), and the existence of phase separation in this lipid mixture is a subject of intensive debate (34–37). Nonetheless, a significant number of experimental and theoretical data support POPC/Chol phase separation into l_d/l_o domains (29,35,38–41). Two factors that might hinder identification of the l_o phase by fluorescence microscopy are 1) a domain size smaller than the diffraction limit, in similarity to l_o domains formed by DPPC/Chol that display a size in the range of 20 nm (42), and/or 2) the looser packing of the POPC/Chol-enriched l_o phase, which is less ordered than a Chol/SM-enriched l_o phase (23,29). This enables the partition of Rho-DOPE into the more ordered fluid phase, preventing identification of the two phases using the NBD/Rho fluorescent-probe pair (43).

Interestingly, our microscopy studies further revealed that the POPC/Chol mixtures displayed a higher tendency to aggregate at acidic pH, suggesting that these mixtures are less stable upon acidification. This was not observed at neutral pH, probably due to the more negative surface charge of the vesicles, which increases electrostatic repulsion, preventing vesicle aggregation.

To study the interplay between Chol and C16-GlcCer, we employed two strategies: 1) the POPC content of the mixtures was held constant and the ratio between C16-GlcCer and Chol was altered, and 2) the ratio between POPC and Chol was kept constant and the content of C16-GlcCer was increased.

Ternary mixtures with different C16-GlcCer/Chol ratios

In the first set of experiments, the POPC concentration was 40 or 70 mol % and the ratio of C16-GlcCer and Chol was varied. The results demonstrated an increase in t-PnA fluorescence anisotropy (Fig. 2 A), mean fluorescence lifetime (Fig. 2 B), and long-lifetime component (Fig. 2 C) upon an increase in C16-GlcCer content, demonstrating the ability of this lipid to increase the packing of the fluid membrane. Membrane order was higher at neutral pH than at acidic pH, as shown by the higher anisotropy and lifetime at pH 7.4. This is in agreement with our previous study
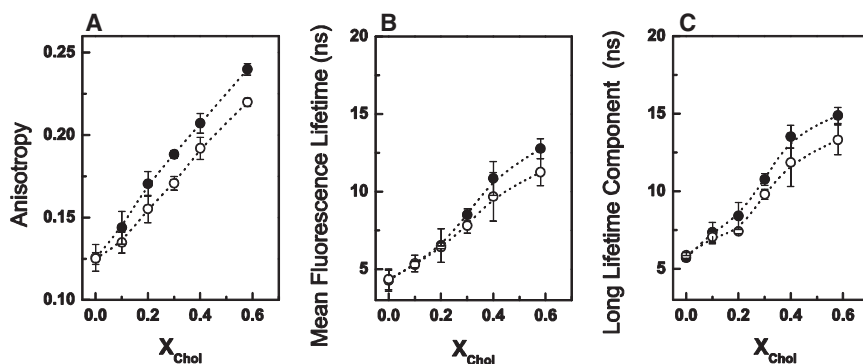

FIGURE 1 Biophysical characterization of POPC/Chol mixtures at different pH values. (A–C) t-PnA (A) fluorescence anisotropy, (B) mean fluorescence lifetime, and (C) long-lifetime component of the intensity decay in binary POPC/Chol mixtures. Measurements were performed at neutral (*solid symbols*) and acidic (*open symbols*) pH. Values are means ± SD of at least three independent experiments.
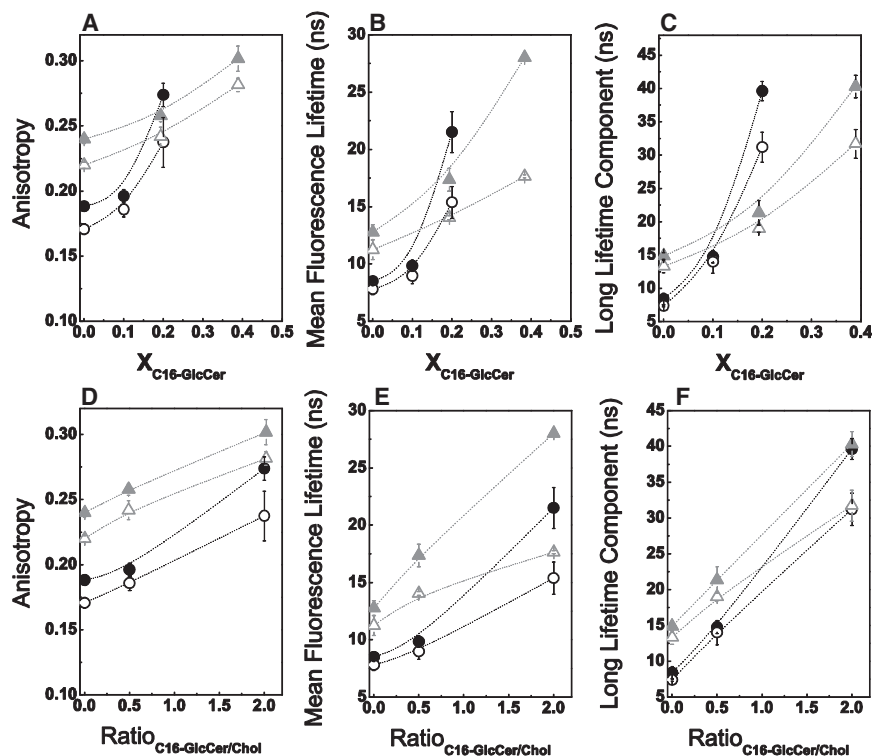
FIGURE 2 Biophysical behavior of POPC/Chol/C16-GlcCer mixtures containing a constant POPC composition. (*A–F*) t-PnA (*A* and *D*) fluorescence anisotropy, (*B* and *E*) mean fluorescence lifetime, and (*C* and *F*) long-lifetime component of t-PnA intensity decay in ternary POPC/Chol/C16-GlcCer mixtures, as a function of (*A–C*) the C16-GlcCer molar fraction or (*D–F*) the C16-GlcCer/Chol ratio. The mixtures contain 40 (*triangles*) or 70 (*circles*) mol % of POPC. Measurements were performed at pH 7.4 (*solid symbols*) and pH 5.5 (*open symbols*). Values are means ± SD of at least three independent experiments.

showing that C16-GlcCer forms more tightly packed domains at neutral pH ([16](16)).

To test whether the increase in packing was dependent on C16-GlcCer levels or also modulated by the interplay between C16-GlcCer and Chol, we plotted the data as a function of the GlcCer/Chol ratio (Fig. 2, *D–F*). For the same POPC content, an increase in the ratio of C16-GlcCer/Chol resulted in an almost linear increase in the anisotropy and fluorescence lifetime of t-PnA, illustrating that the membrane becomes more ordered as the C16-GlcCer content is increased. A comparison between mixtures containing different POPC content showed that with a decrease in POPC content, there was a strong increase in the fluorescence anisotropy (Fig. 2 *D*) and mean fluorescence lifetime (Fig. 2 *E*) of t-PnA irrespective of the C16-GlcCer/Chol ratio, whereas the long-lifetime component of t-PnA was similar for mixtures containing a higher C16-GlcCer/Chol ratio (Fig. 2 *F*). The fluorescence anisotropy and mean fluorescence lifetimes are ensemble average values that depend on the partition properties of the probe with regard to the different phases present in the lipid mixtures, as well as on the fraction of each phase. In contrast, the long-lifetime component provides information about the packing properties of the more ordered phases and is independent on the amount of phase that is present. Therefore, these results suggest that with a decrease in the POPC content, there is an increase in the fraction of the ordered phase (Fig. 2, *D* and *E*). However, the packing properties of the mixtures are similar (Fig. 2 *F*), suggesting that for these

particular mixtures, only the fraction of the ordered phase changes and thus should correspond to a tie-line in the phase diagram.

For the ternary mixtures in which the C16-GlcCer content exceeds that of Chol, both the anisotropy and lifetime of t-PnA are high and typical of a C16-GlcCer-enriched gel phase ([16](16)). This is further supported by the detailed analysis of the lifetime components of t-PnA fluorescence intensity decay (Fig. S3): the presence of gel-fluid phase separation is characterized by the requirement of a fourth component to describe the fluorescence intensity decay of the probe (Fig. S3) ([23,33](23,33)). The lower long-lifetime component at pH 5.5 (Figs. 2, *C* and *F*, and S3 *B*) further supports the evidence that membrane packing is decreased upon acidification ([21](21)).

To further characterize these mixtures, fluorescence microscopy studies were performed (Fig. 3). Increasing the C16-GlcCer content of the mixtures drove phase separation into ordered (*dark*) and disordered (*bright*) regions. The irregular shape of the domains, together with the exclusion of the probes from those areas, suggests that they correspond to gel-phase domains, in agreement with the spectroscopy data (Figs. 2 and S3). The effect of the pH on the shape and size of the domains was not significant. However, a strong tendency for vesicular fusion and tubule formation was observed at acidic pH in vesicles containing ≥20 mol % of C16-GlcCer (Figs. 3 and S4).

To better characterize the size heterogeneity of the vesicle population, DLS was performed (Fig. S5). An increase in
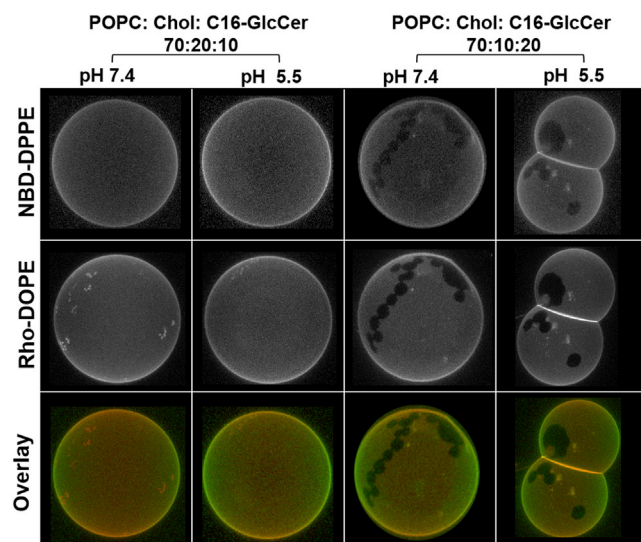
FIGURE 3 Confocal fluorescence microscopy of POPC/Chol/C16-GlcCer mixtures with constant POPC levels. 3D projection images from 0.4 μm confocal slices of POPC/Chol/C16-GlcCer GUVs labeled with NBD-DPPE and Rho-DOPE at neutral and acidic pH. Scale bar, 5 μm.

the mean diameter of the vesicles was observed at acidic pH, particularly for mixtures containing 40% POPC (Fig. S5 A). This was accompanied by high scattering intensities recorded in the range of 0.5−5.5 μm (Fig. S5, B and C), demonstrating that at acidic pH, the vesicles have a higher tendency to fuse and/or form tubular structures that result in an increased PdI (Fig. S5 D). In addition, the results showed that both the mean diameter (Fig. S5 A) and PdI (Fig. S5 D) increased upon elevation of C16-GlcCer content in the mixtures, particularly at pH 5.5. To test whether this effect was mainly due to the presence of C16-GlcCer, binary POPC/C16-GlcCer mixtures were also analyzed (Fig. S6). As was observed for the ternary POPC/Chol/C16-GlcCer mixtures, an increase in the C16-GlcCer content of the binary POPC/C16-GlcCer mixtures resulted in an increase in the mean diameter of the vesicles (Fig. S6 A). However, the shift in the scattering intensity toward a larger vesicle population (Fig. S6, B and C) and the elevation of the PdI of the vesicles (Fig. S6 D) were higher at pH 5. These results are consistent with an increased ability of the vesicles to alter their shape (Fig. 3) and undergo tubule formation (Fig. S4) upon an increase in C16-GlcCer content (16,21). The higher instability of both the binary and ternary lipid vesicles at acidic pH may be a consequence of a change in the surface charge upon a change in the pH environment (Figs. S5 E and S6 E). Indeed, at acidic pH, the net surface charge is close to neutral, which results in a decrease in the electrostatic repulsive forces between the vesicles, favoring their aggregation.

Since the binary and ternary results reveal similar behaviors, we suggest that C16-GlcCer is the main element affecting the membrane properties.

Ternary mixtures with a constant POPC/Chol ratio

In the second set of experiments, the ratio between POPC/Chol was kept constant to mimic a binary mixture, with 25% and 75% of l_o phase. The composition of these mixtures was determined based on the POPC/Chol phase diagram (29) and correspond to POPC/Chol molar ratios of 79/21 and 62/38, respectively. The content of C16-GlcCer in these mixtures was then varied from 0 to 30 mol % and studies were performed at both neutral and acidic pH. In the absence of C16-GlcCer and for mixtures containing 10 mol % C16-GlcCer, the t-PnA fluorescence anisotropy (Fig. 4, A and B) and mean fluorescence lifetime (Fig. 4, C and D) were higher for mixtures where the POPC/Chol ratio mimicked 75% of l_o phase, reflecting the larger l_o phase fraction of these mixtures compared with a POPC/Chol ratio mimicking 25% of the l_o phase (29,38). Moreover, both the t-PnA fluorescence anisotropy and mean fluorescence lifetime steadily increased with an increasing content of C16-GlcCer in both sets of ternary mixtures, irrespective of the pH. In addition, the photophysical parameters of t-PnA showed a larger variation in mixtures with a lower Chol content, i.e., mixtures with a
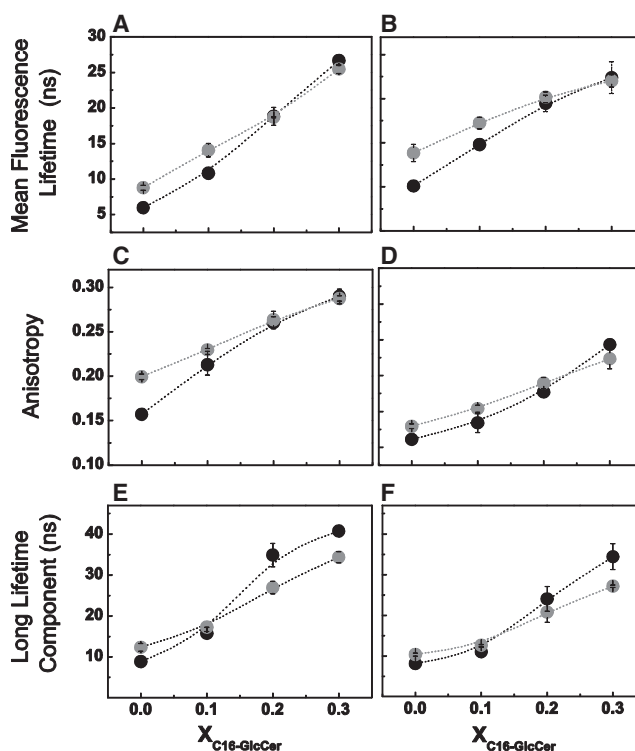

FIGURE 4 Biophysical characterization of POPC/Chol/C16-GlcCer mixtures with a constant POPC/Chol ratio. (A–F) t-PnA (A and B) fluorescence anisotropy, (C and D) mean fluorescence lifetime, and (E and F) long-lifetime component of the intensity decay in ternary POPC/Chol/C16-GlcCer mixtures with POPC/Chol ratios mimicking 25 (*black circles*) and 75 (*gray circles*) mol % of an l_o phase. Measurements were performed at (A, C, and E) neutral and (B, D, and F) acidic pH. Values are means ± SD of at least three independent experiments.

POPC/Chol ratio mimicking 25% of l_o phase, demonstrating that C16-GlcCer induces stronger changes in a membrane that contains a larger fraction of l_d phase. No significant differences in the global order of the membrane were detected between the two sets of ternary mixtures when C16-GlcCer was ≥ 20 mol %, as shown by the similar t-PnA fluorescence anisotropy (Fig. 4, A and B) and mean fluorescence lifetime (Fig. 4, C and D) values. However, the packing properties of the more-ordered phase changed when the lipid composition of the mixtures was varied (Fig. 4, E and F). In the absence of C16-GlcCer, the long-lifetime components of the t-PnA fluorescence intensity decay were similar for the two sets of ternary mixtures, showing identical packing properties of the l_o phase, as would be anticipated for mixtures located within the same tie-line (29). With increasing C16-GlcCer content, the lifetime component of t-PnA became longer and increased to a higher extent for mixtures with a lower Chol content. The results suggest that mixtures in which the POPC/Chol ratio mimics 25% of l_o phase have a higher extent of gel-fluid phase separation than those in which the POPC/Chol ratio mimics 75% of l_o phase. An analysis of the lifetime components of the t-PnA fluorescence intensity decay further supports this conclusion, as shown by the increase in the preexponential associated with the longest lifetime component (Fig. S7, A, C, E, and G) and the requirement for four components to describe the fluorescence intensity decay of t-PnA for mixtures containing ≥ 20 mol % C16-GlcCer, which are indicative of gel-fluid phase separation (Fig. S7, B, D, F, and H).

The effect of C16-GlcCer on the global membrane order and packing properties of the mixtures is more pronounced at neutral pH than at acidic pH (Figs. 4 and S8), as shown by the higher fluorescence anisotropy (Fig. S8, A and D), mean fluorescence lifetime (Fig. S8, B and E), and longer lifetime component of the t-PnA fluorescence intensity decay (Fig. S8, C and F). These results are consistent with the greater ability of C16-GlcCer to change its membrane-packing properties at neutral pH than at acidic pH (21).

Microscopy studies further supported the conclusions we drew from the spectroscopy studies: the extent of gel-fluid phase separation was higher for mixtures containing ≥ 20 mol % C16-GlcCer when the POPC/Chol ratio mimicked 25% of l_o phase (Fig. 5 A) compared with 75% of l_o phase (Fig. 5 B). In addition, l_d/l_o phase separation was also observed in ternary mixtures with a lower C16-GlcCer content and/or higher Chol content (Fig. 5, mixtures with 10 mol % of C16-GlcCer). This is shown by the presence of round-shaped domains that only partially exclude the probes. These results suggest that C16-GlcCer interacts with Chol to form a more tightly packed l_o phase that can be distinguished by fluorescence microscopy using NBD-DPPE and Rho-DOPE as probes. Phase separation into l_d, l_o, and gel phases was observed for mixtures containing 20 and 30 mol % of C16-GlcCer and a POPC/Chol ratio mimicking 25% of l_o phase (Fig. 5 A). Indeed, a layer enriched in the NBD-DPPE
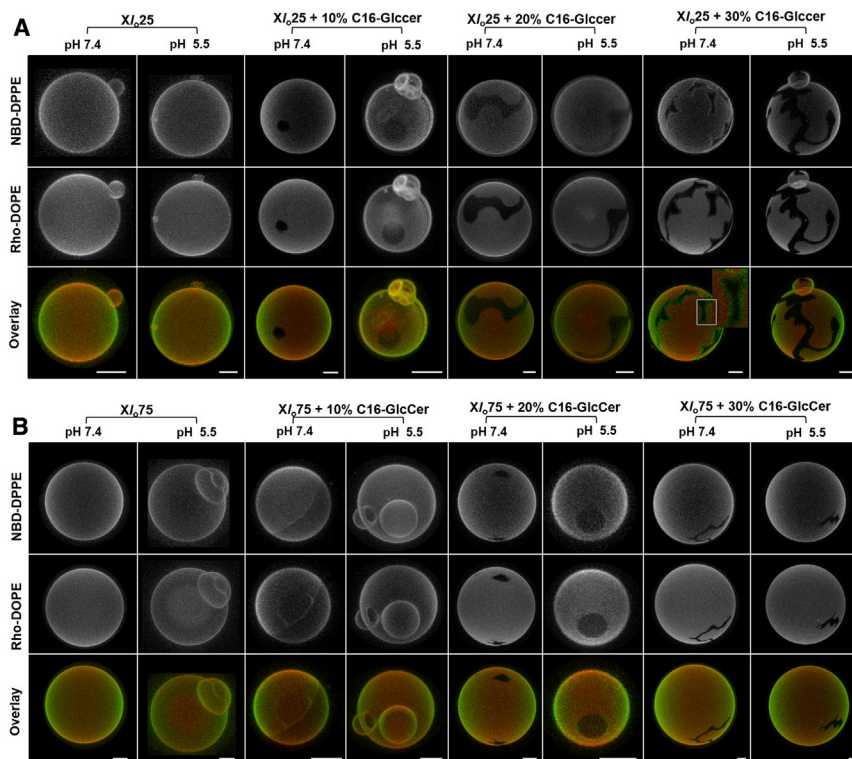

FIGURE 5 Confocal fluorescence microscopy of POPC/Chol/C16-GlcCer GUVs with a constant POPC/Chol ratio. 3D projection images from 0.4 μm confocal slices of GUVs with POPC/Chol ratios mimicking (A) 25 and (B) 75 mol % of the l_o phase and increasing molar fractions of C16-GlcCer. GUVs were labeled with NBD-DPPE and Rho-DOPE. Studies were performed at neutral and acidic pH. Scale bar, 5 μm.

probe surrounding the gel domain was observed, suggesting that this l_o-enriched phase in the interface of the gel and fluid phase promotes a subtle transition, avoiding the high line tension arising from a typical gel-fluid phase separation.

A stronger tendency for vesicle aggregation, fusion, and tubule formation was again observed at acidic pH (Figs. 5 and S4). Analyses of the vesicle population by DLS showed a higher mean diameter (Fig. S9 A) and PdI of the vesicles (Fig. S9 B), and an increase in the scattering intensities in the range of $0.5-6$ μm at acidic pH compared with neutral pH (Fig. S9, C–F). In addition, the differences were more pronounced upon an increase in the C16-GlcCer content of the mixtures at pH 5.5, which may be related to the ability of C16-GlcCer to induce shape transformation of the vesicles under acidic conditions. The higher instability of the vesicle population at acidic pH may also be related to a decreased electrostatic repulsion between vesicles due to a net surface charge close to neutrality (Fig. S9 G). The results further demonstrate that at neutral pH the net surface charge is negative, contributing to a higher electrostatic repulsion and preventing a strong interaction between the vesicles that would contribute to their aggregation and/or fusion.

DISCUSSION

GlcCer has been implicated in the formation of lipid domains, particularly in the so-called lipid raft domains, but the interplay between GlcCer and Chol has not been studied in detail. In this work, we aimed to provide further insight into the interactions between these two key membrane lipids and how they change the biophysical properties of fluid phospholipid membranes. Moreover, we sought to evaluate how these interactions are modified by environmental factors, such as changes in pH, considering that accumulation of GlcCer in acidic compartments occurs under pathological conditions, particularly in Gaucher disease (44). Increased levels of GlcCer may lead to alterations in membrane properties and compromise the integrity of the lysosomal membrane. Thus, it is important to understand the biophysical behavior of this lipid under conditions that mimic its subcellular distribution.

Qualitative analysis of the interplay between GlcCer and Chol

Overall, our results demonstrate that ternary mixtures with a higher Chol/GlcCer ratio display properties typical of the l_o phase, whereas decreasing the ratio of these lipids leads to gel-fluid phase separation. This behavior is similar to that observed for mixtures containing Chol and ceramides, although a larger amount of GlcCer is required to induce gel-phase formation compared with mixtures containing ceramides (23). Previous studies performed by Maunula et al. (17) in a mixture containing Chol and GlcCer showed that

GlcCer partitioning into sterol-enriched domains was low. These results are consistent with our findings in this study, since mixtures containing a high GlcCer/Chol ratio, such as the one used by Maunula et al. (17), display a strong tendency to form gel domains.

The ability of GlcCer to induce gel-fluid phase separation on the ternary mixtures was reduced upon acidification of the environment, similar to what was observed in POPC/GlcCer mixtures (21).

Moreover, GlcCer-induced vesicle aggregation and shape transformation were increased at pH 5.5, as shown by both microscopy and vesicle-size analysis. This tendency is most likely associated with the overall surface charge of the vesicles, which is close to neutrality at acidic pH. The same behavior was observed for vesicles containing $\geq$20 mol % Chol, where increased aggregation and decreased electronegativity of the vesicles were observed. Previous studies also showed that liposomes containing Chol had a tendency to fuse and aggregate at acidic pH (45,46).

Interestingly, mixtures containing Chol, GlcCer, or both lipids showed a concentration-dependent decrease in the overall surface charge of the vesicles, even though no change in the net charge of these lipids is expected, since the pKa of the acidic groups of Chol and GlcCer is ~16 and 12 (Fig. 6 D) (21,47), respectively. Note that no significant changes in the surface charge of POPC vesicles were observed after a change from neutral to acid pH, indicating that variation in the ZP is related to the Chol- and GlcCer-vesicle composition.

It is assumed that the usual pKa of a fatty acid in water shifts from pKa ~5 to pKa ~7 upon interaction with a membrane, reflecting the strong change in the environment. However, since the hydroxyl group is not near the double-conjugated bonds, it is not expected that alterations in the ionization state of the probe that could occur at pH 5.5 would affect the fluorescence properties of this lipid probe. However, ionization could influence the probe location in the membrane, which could result in changes in its photophysical properties, particularly the fluorescence anisotropy and lifetime. According to the Perrin equation, anisotropy combines information about both the fluorescence lifetime and the medium viscosity/rigidity, and, in addition, is not based on the absolute fluorescence intensities, which would be dependent on the probe concentration and more prone to error. Therefore, to check whether the ionization state of the probe was influencing either the probe location or its photophysical properties, we evaluated the trend of variation in the t-PnA fluorescence anisotropy upon a variation in pH, as well as the buffer composition in mixtures containing different GlcCer molar ratios. Under these conditions, both the ionic strength and the cation/anion concentration of the citrate-phosphate buffer increased as the pH increased (Table S1). Moreover, although citrate-phosphate buffer at pH 7.4 is significantly different from PBS buffer at the same pH, the anisotropy values for t-PnA in mixtures
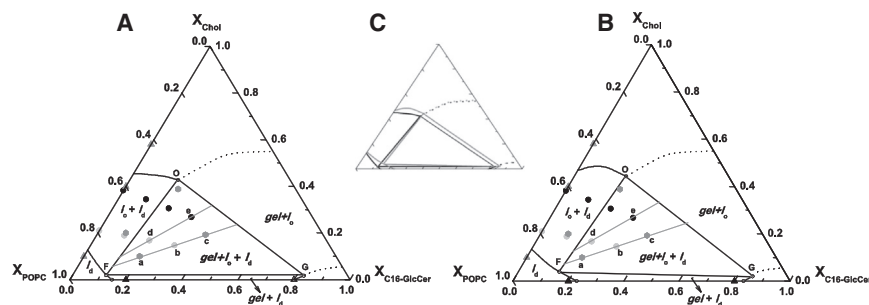
FIGURE 6 Partial ternary phase diagram of POPC/Chol/C16-GlcCer mixtures. (*A* and *B*) POPC/Chol/C16-GlcCer partial ternary phase diagrams at 24°C and (*A*) neutral and (*B*) acidic pH. The diagrams were determined using the photophysical properties of t-PnA and microscopy data. Solid symbols are experimental data for the following mixtures: POPC/Chol (*gray triangles*), POPC/GlcCer (*black triangles*), POPC/Chol/C16-GlcCer ternary systems with a constant POPC fraction (*dark gray hexagons*), and POPC/Chol/C16-GlcCer with a constant POPC/Chol ratio mimicking 25 (*light gray circles*) and 75 mol % of the l_o phase (*black circles*). The boundaries of the tie-triangle and the coexisting l_o+l_d phase are based on a mathematical analysis of the experimental data (see Table S2 and Supporting Material). The data for POPC/GlcCer were taken from Varela et al. (16), and the data for POPC/Chol mixtures were complemented by data from de Almeida et al. (29). The dashed lines on the right side of the ternary diagrams are just illustrative of the possible boundaries of the $g+l_o$ phase. (*C*) Overlap of the diagrams shows a shift of the tie-triangle to higher GlcCer molar fractions at acidic pH (in *gray*) compared with neutral pH (in *black*). All of the lines have a strong experimental basis and are thermodynamically consistent.

prepared with these buffers are identical (Fig. S10) irrespective of the lipid composition of the mixtures. This shows that the changes observed in t-PnA anisotropy upon a change in the pH of the ternary POPC/Chol/GlcCer mixtures were not due to pH variation or to compositional differences of the buffer. Moreover, an increase in t-PnA anisotropy with an increase in buffer pH was only observed for mixtures displaying a gel-fluid phase transition, i.e., containing 30 mol % GlcCer. This further supports the assumption that changes in the pH environment mainly affect the organization of GlcCer molecules involved in the formation of the gel phase, as we previously suggested (21). Therefore, our results suggest that important alterations take place at the surface of the vesicles upon a change in pH.

In a recent study, Magarkar et al. (48) reported that increasing the Chol content in POPC/Chol mixtures resulted in an increase in the electronegativity of the vesicles, which was explained based on a decreased binding of Na^+ ions to the surface of the vesicles. This phenomenon was due to the lower ability of Na^+ ions to interact with Chol hydroxyl (OH) groups compared with phosphatidylcholine (PC) headgroups. Moreover, the authors suggested that the increased association between Chol-OH groups and PC headgroups, and increased membrane hydrophobicity upon an increase in Chol content also contributed to an overall decrease in the number of binding sites for cations (48). It is possible that similar alterations take place in GlcCer-containing vesicles, particularly when one considers the strong ability of GlcCer to establish an H-bond network. Increased H-bonding will contribute to a decrease in the layer of positive ions (such as Na^+ or H^+) interacting with the vesicle surface. These observations may also help to explain why the ability of GlcCer and Chol to increase the order of the membranes is decreased at acidic pH. Indeed, under acidic conditions, the surface charge of Chol-, GlcCer-, and Chol/GlcCer-containing mixtures is close to that obtained for POPC vesicles, suggesting that the number of ions bound to the surface is constant. This suggests that

the polar groups of Chol and GlcCer experience conformational changes that might contribute to their lower exposure and/or compromised ability to establish H-bonds with the phospholipids, in agreement with our previous study (21). It is possible that an increase in H^+ content, as observed at acidic pH, might contribute to a higher extent of H-bond networks between the lipids and the solvent, to the detriment of lipid-lipid H-bonds. This would certainly contribute to a decrease in the packing of the lipids and therefore a decrease in the overall membrane order upon acidification.

Determination of a POPC/Chol/GlcCer partial ternary phase diagram

Together with previous data, our results allowed us to determine a partial ternary phase diagram that quantitatively describes the interplay between GlcCer and Chol in a fluid POPC matrix. POPC/Chol (29) and POPC/GlcCer (16) binary phase diagrams were used to establish the boundaries that define the l_d/l_o (*gray triangles*) and gel/fluid phase (*black triangles*) separation for these binary mixtures (Fig. 6). Moreover, thermodynamic principles such as the phase rule and limitations to the two-phase/one-phase boundaries imposed by the Gibbs energy minimum principle (49,50) were taken into account. All of the experimental data were analyzed, and the fraction of each phase that was present in a given mixture was determined as described previously (51). This methodology considers the partition coefficient (K_p) of the probe between each phase and the experimental photophysical parameters of the probe in each pure phase, as well as in the lipid mixtures displaying phase coexistence. The methodology is explained in detail in the appendix section of Castro et al. (51) and in Supporting Materials and Methods.

Table 1 shows a summary of the partition coefficients of t-PnA for a given phase. K_p values were determined using the variation of the fluorescence anisotropy and/or mean

TABLE 1   Partition Coefficient of t-PnA in Different Lipid Mixtures and between Different Phases

Lipid Mixtures	pH 7.4 ($\leq \pm 0.0005$)	pH 5.5 ($\leq \pm 0.010$)
$K_p^{g/ld}$ in POPC/C16-GlcCer	4.70	2.47
$K_p^{lo/ld}$ in POPC/Chol	0.14	0.14
$K_p^{g/lo}$ in POPC/Chol/C16-GlcCer	34.40	17.64

fluorescence lifetime of t-PnA as a function of the phase fraction in the indicated binary mixtures (see Supporting Materials and Methods). $K_p^{g/lo}$ was obtained from the ratio of the $K_p^{g/ld}$ and $K_p^{lo/ld}$ of t-PnA (51). The values indicate that t-PnA has a very high preference for the GlcCer-enriched gel phase in comparison with the l_d and l_o phases.

Using the different K_p values, we were able to determine the fraction of each phase for all of the studied mixtures (Table S2). As could be anticipated, mixtures with a lower Chol content, such as those mimicking 25% of l_o phase, had a larger fraction of gel phase. The fraction of gel phase was always lower at pH 5.5 than at pH 7.4.

After determining the phase fractions, we used an iterative method to estimate the boundaries of the partial ternary phase diagram (52). Briefly, we assayed different configurations for a phase diagram of the type shown in Fig. 6, and computed the phase fractions and compositions. We then compared these results with the experimental values. The iteration that provided the smaller maximal difference between the experimental data and the calculated values is shown in Fig. 6 (see Supporting Materials and Methods for additional details). Note that only the left part of the diagram was experimentally assessed, since this corresponds to more physiological conditions, i.e., high phospholipid content and low-to-medium Chol and GlcCer content. This area of the diagram consists of four different regions corresponding to relatively small areas of 1) POPC-enriched fluid (l_d), 2) POPC-enriched fluid + GlcCer-enriched gel ($l_d + g$), 3) an intermediate POPC-enriched l_d + Chol-enriched l_o ($l_d + l_o$) region, and 4) a large POPC-enriched l_d + Chol-enriched l_o + GlcCer-enriched gel ($l_d + l_o + g$). This region, defined by a broad tie-triangle, denotes the relatively high immiscibility between the three lipid components. The tie-lines inside the tie-triangle were determined by analysis of the experimental data, particularly the fluorescence spectroscopy measurements. Indeed, the three samples (a, b, and c) crossed by the tie-line display identical packing properties, as shown by similar t-PnA long-lifetime components for the three mixtures at pH 7.4 (~40 ns) and pH 5.5 (~32 ns). The same was observed for the second tie-line, crossing samples d and e, where the t-PnA long-lifetime components of the mixtures were ~34 ns and ~27 ns, at pH 7.4 and 5.5, respectively. This evidence shows that the properties of the phases are identical for the different mixtures in each of the tie-lines, and only the fraction of the phases is changing (Table S2), which is in agreement with the definition of a tie-line.

The right side of the diagram was not experimentally determined. However, using thermodynamic considerations, it is possible to predict the orientation of the boundaries. The two-phase region should cross the ternary phase with a similar slope and extend inside the three-phase region (49,50). Therefore, to respect the geometric constraints imposed by the presence of the three-phase region, the points that define the top and lower right of the tie-triangle connect the right side of the ternary diagram, with a line displaying a positive slope (50). However, it is not possible to predict the composition at which g/l_o phase coexistence occurs for Chol/GlcCer mixtures, and therefore those boundaries are merely illustrative (Fig. 6).

Compared with POPC/SM/Chol mixtures (29), this diagram presents a smaller region with l_o/l_d phase coexistence. It can therefore be concluded that GlcCer has a lower miscibility in the l_o phase compared with SM. This is likely due to both the high melting temperature of GlcCer and its stronger tendency to segregate into tightly packed gel domains (16,18,20). A comparison of the POPC/Chol/C16-GlcCer and POPC/Chol/C16-Cer partial phase diagrams allows us to conclude that the presence of the glucose moiety in the headgroup of GlcCer increases the miscibility of GlcCer in the l_o phase compared with Cer (7,23). This suggests that significant levels of GlcCer may be involved in the formation of l_o domains in more complex biological membranes. However, very small fractions of Cer are sufficient to perturb the biophysical properties of l_o domains and drive gel-fluid phase separation (33). Indeed, the POPC/Chol/C16-Cer phase diagram (23) exhibits relevant differences in comparison with the POPC/Chol/C16-GlcCer ternary phase diagram. Although the solubility of C16-Cer in a Chol-enriched fluid phase is minimal, leading to a very large gel/fluid phase separation region, GlcCer is capable of interacting with the Chol-forming l_o phase (23,53). The difference in behavior between the two lipids is probably due to the nature of the interaction of Cer and GlcCer with the neighboring lipids. C16-Cer promotes very strong intermolecular bonds, forming domains with a very high packing density (23,54,55), which hinders the incorporation of Chol into the membrane. In contrast, the size of the sugar residue in C16-GlcCer might preclude the formation of domains with an equivalent packing density, which might facilitate the interaction of GlcCer with Chol (17,21).

It is worth mentioning that even a minor alteration in the headgroup of the SLs is enough to significantly alter the interplay established between the SL and Chol. For example, in comparison with galactosylceramide (GalCer), which only differs from GlcCer regarding the position of the OH group, GlcCer-enriched domains are able to incorporate more Chol. This is probably due to the strength of the intermolecular interactions, which are stronger in GalCer, hindering Chol incorporation into GalCer-enriched domains (17).

The effect of pH on the interplay between POPC/Chol and GlcCer was also translated into a partial ternary phase diagram. A comparison of the two diagrams shows a slightly broader coexistence between the l_o and l_d phases at acidic pH. This shows that GlcCer miscibility in the l_o phase is increased upon acidification, and suggests that the l_o domains can accommodate higher levels of GlcCer under acidic conditions without significantly changing the properties of the l_o phase (Fig. 6 B). In a biological context, the subtle differences in the phase behavior of the mixtures at different pH values could be enough to induce a large perturbation in membrane organization, particularly considering that alterations in membrane packing and organization are accompanied by a strong tendency to induce membrane fusion/aggregation upon acidification. From a biological perspective, such alterations might impact a number of membrane fusion events, including those associated with vesicle trafficking (56,57). In other words, in a complex system like a natural cell membrane, a slight change in membrane properties could have a cascade effect, leading to membrane distortions that could affect, for instance, protein conformation, ultimately altering cell responses.

CONCLUSIONS

GlcCer is one of several bioactive lipids that modulate cell signaling, possibly by inducing the formation of membrane domains. Our rationale for designing this study was the lack of systematic biophysical analyses to explore the interactions between GlcCer and another critical lipid involved in lipid domain formation, namely, Chol.

The partial POPC/Chol/GlcCer ternary phase diagram obtained in this study complements previous studies using similar mixtures (22) and provides a valuable tool for future studies, e.g., to quantitatively analyze alterations in the phase behavior of these mixtures upon interaction with relevant molecules, such as proteins or drugs. Phase diagrams are also indispensable for studies that address lipid-protein interactions and protein partitioning into lipid domains. These phase diagrams will enhance our understanding of how the interplay between these lipids might affect the distribution and sorting of different proteins. The qualitative and quantitative analyses of the phase properties of these mixtures constitute a further step toward understanding the lipid-lipid interactions and membrane biophysical properties in complex biological membranes. As an example, a comparison of these and other SL/Chol-phase diagrams (23,29) might allow investigators to predict the biophysical changes that occur in membrane properties upon metabolic conversion of one SL species into another. Since several SL species are involved in signaling events, integrative analyses based on biophysical and biological studies might help to elucidate the link between the biophysical properties of these lipids and their biological functions.

AUTHOR CONTRIBUTIONS

L.C.S. conceived the study. L.C.S. and A.R.P.V. designed the experiments. A.R.P.V., A.S.C., A.F., and L.C.S. performed the experiments and data analysis. All authors discussed the results and the implications. A.R.P.V., A.H.F., M.P., and L.C.S. wrote the manuscript.

REFERENCES

1. Okazaki, T., R. M. Bell, and Y. A. Hannun. 1989. Sphingomyelin turn-over induced by vitamin D3 in HL-60 cells. Role in cell differentiation. *J. Biol. Chem.* 264:19076–19080.

2. Spiegel, S., and S. Milstien. 2003. Sphingosine-1-phosphate: an enigmatic signalling lipid. *Nat. Rev. Mol. Cell Biol.* 4:397–407.

3. Hannun, Y. A., and L. M. Obeid. 2008. Principles of bioactive lipid signalling: lessons from sphingolipids. *Nat. Rev. Mol. Cell Biol.* 9:139–150.

4. Simons, K., and E. Ikonen. 1997. Functional rafts in cell membranes. *Nature.* 387:569–572.

5. Gulbins, E., and P. L. Li. 2006. Physiological and pathophysiological aspects of ceramide. *Am. J. Physiol. Regul. Integr. Comp. Physiol.* 290:R11–R26.

6. Castro, B. M., M. Prieto, and L. C. Silva. 2014. Ceramide: a simple sphingolipid with unique biophysical properties. *Prog. Lipid Res.* 54:53–67.

7. Goñi, F. M., and A. Alonso. 2009. Effects of ceramide and other simple sphingolipids on membrane lateral structure. *Biochim. Biophys. Acta.* 1788:169–177.

8. de Almeida, R. F., J. T. Marquês, and L. C. Silva. 2014. Biophysics of lipid rafts and their interplay with ceramide: studies in model systems and biological insights. *In* Lipid Rafts: Properties, Controversies and Roles in Signal Transduction. D. Sillence, editor. Nova Science Publishers, New York, pp. 21–36.

9. Hakomori, S. I. 2010. Glycosynaptic microdomains controlling tumor cell phenotype through alteration of cell growth, adhesion, and motility. *FEBS Lett.* 584:1901–1906.

10. Parton, R. G. 1994. Ultrastructural localization of gangliosides; GM1 is concentrated in caveolae. *J. Histochem. Cytochem.* 42:155–166.

11. Degroote, S., J. Wolthoorn, and G. van Meer. 2004. The cell biology of glycosphingolipids. *Semin. Cell Dev. Biol.* 15:375–387.

12. Zhang, W., B. Quinn, S. Barnes, G. Grabowski, and Y. Sun. 2013. Metabolic profiling and quantification of sphingolipids by liquid chromatography-tandem mass spectrometry. *J. Glycomics Lipidomics.* 3:107.

13. Ramstedt, B., and J. P. Slotte. 2002. Membrane properties of sphingomyelins. *FEBS Lett.* 531:33–37.

14. Lloyd-Evans, E., D. Pelled, …, A. H. Futerman. 2003. Glucosylceramide and glucosylsphingosine modulate calcium mobilization from brain microsomes via different mechanisms. *J. Biol. Chem.* 278:23594–23599.

15. Sillence, D. J., V. Puri, …, F. M. Platt. 2002. Glucosylceramide modulates membrane traffic along the endocytic pathway. *J. Lipid Res.* 43:1837–1845.

16. Varela, A. R. P., A. M. P. S. Gonçalves da Silva, …, L. C. Silva. 2013. Effect of glucosylceramide on the biophysical properties of fluid membranes. *Biochim. Biophys. Acta.* 1828:1122–1130.

17. Maunula, S., Y. J. E. Björkqvist, …, B. Ramstedt. 2007. Differences in the domain forming properties of N-palmitoylated neutral glycosphingolipids in bilayer membranes. *Biochim. Biophys. Acta.* 1768:336–345.

18. Westerlund, B., and J. P. Slotte. 2009. How the molecular features of glycosphingolipids affect domain formation in fluid membranes. *Biochim. Biophys. Acta.* 1788:194–201.

19. Maggio, B., D. C. Carrer, …, C. M. Rosetti. 2004. Interfacial behavior of glycosphingolipids and chemically related sphingolipids. *Curr. Opin. Colloid Interface Sci.* 8:448–458.

20. Saxena, K., R. I. Duclos, …, G. G. Shipley. 1999. Structure and properties of totally synthetic galacto- and gluco-cerebrosides. *J. Lipid Res.* 40:839–849.

21. Varela, A. R. P., A. M. P. S. Gonçalves da Silva, …, L. C. Silva. 2014. Influence of intracellular membrane pH on sphingolipid organization and membrane biophysical properties. *Langmuir.* 30:4094–4104.

22. Slotte, J. P., A. L. Ostman, …, R. Bittman. 1993. Cholesterol interacts with lactosyl and maltosyl cerebrosides but not with glucosyl or galactosyl cerebrosides in mixed monolayers. *Biochemistry.* 32:7886–7892.

23. Castro, B. M., L. C. Silva, …, M. Prieto. 2009. Cholesterol-rich fluid membranes solubilize ceramide domains: implications for the structure and dynamics of mammalian intracellular and plasma membranes. *J. Biol. Chem.* 284:22978–22987.

24. Almeida, P. F. F., A. Pokorny, and A. Hinderliter. 2005. Thermodynamics of membrane domains. *Biochim. Biophys. Acta.* 1720:1–13.

25. McClare, C. W. F. 1971. An accurate and convenient organic phosphorus assay. *Anal. Biochem.* 39:527–530.

26. Sklar, L. A., B. S. Hudson, …, J. Diamond. 1977. Conjugated polyene fatty acids on fluorescent probes: spectroscopic characterization. *Biochemistry.* 16:813–819.

27. R. P. Haugland, M. T. Spence, and I. D. Johnson, editors 1996. Handbook of Fluorescent Probes and Research Chemicals. Molecular Probes, Eugene, OR.

28. Birch, D. S., and R. Imhof. 2002. Time-domain fluorescence spectroscopy using time-correlated single-photon counting. *In* Topics in Fluorescence Spectroscopy. J. Lakowicz, editor. Springer US, New York, pp. 1–95.

29. de Almeida, R. F. M., A. Fedorov, and M. Prieto. 2003. Sphingomyelin/phosphatidylcholine/cholesterol phase diagram: boundaries and composition of lipid rafts. *Biophys. J.* 85:2406–2416.

30. de Almeida, R. F. M., J. Borst, …, A. J. W. G. Visser. 2007. Complexity of lipid domains and rafts in giant unilamellar vesicles revealed by combining imaging and microscopic and macroscopic time-resolved fluorescence. *Biophys. J.* 93:539–553.

31. Pinto, S. N., L. C. Silva, …, M. Prieto. 2008. Membrane domain formation, interdigitation, and morphological alterations induced by the very long chain asymmetric C24:1 ceramide. *Biophys. J.* 95:2867–2879.

32. Sarmento, M. J., M. Prieto, and F. Fernandes. 2012. Reorganization of lipid domain distribution in giant unilamellar vesicles upon immobilization with different membrane tethers. *Biochim. Biophys. Acta.* 1818:2605–2615.

33. Silva, L. C., R. F. M. de Almeida, …, M. Prieto. 2007. Ceramide-domain formation and collapse in lipid rafts: membrane reorganization by an apoptotic lipid. *Biophys. J.* 92:502–516.

34. Veatch, S. L., and S. L. Keller. 2003. Separation of liquid phases in giant vesicles of ternary mixtures of phospholipids and cholesterol. *Biophys. J.* 85:3074–3083.

35. Frazier, M. L., J. R. Wright, …, P. F. F. Almeida. 2007. Investigation of domain formation in sphingomyelin/cholesterol/POPC mixtures by fluorescence resonance energy transfer and Monte Carlo simulations. *Biophys. J.* 92:2422–2433.

36. Veatch, S. L., and S. L. Keller. 2005. Miscibility phase diagrams of giant vesicles containing sphingomyelin. *Phys. Rev. Lett.* 94:148101.

37. Goñi, F. M., A. Alonso, …, J. L. Thewalt. 2008. Phase diagrams of lipid mixtures relevant to the study of membrane rafts. *Biochim. Biophys. Acta.* 1781:665–684.

38. de Almeida, R. F. M., L. M. S. Loura, …, M. Prieto. 2005. Lipid rafts have different sizes depending on membrane composition: a time-resolved fluorescence resonance energy transfer study. *J. Mol. Biol.* 346:1109–1120.

39. Reyes Mateo, C., A. Ulises Acuña, and J. C. Brochon. 1995. Liquid-crystalline phases of cholesterol/lipid bilayers as revealed by the fluorescence of *trans*-parinaric acid. *Biophys. J.* 68:978–987.

40. Thewalt, J. L., and M. Bloom. 1992. Phosphatidylcholine: cholesterol phase diagrams. *Biophys. J.* 63:1176–1181.

41. Palmieri, B., T. Yamamoto, …, S. A. Safran. 2014. Line active molecules promote inhomogeneous structures in membranes: theory, simulations and experiments. *Adv. Colloid Interface Sci.* 208:58–65.

42. Edidin, M. 2003. Lipids on the frontier: a century of cell-membrane bilayers. *Nat. Rev. Mol. Cell Biol.* 4:414–418.

43. Castro, B. M., R. F. M. de Almeida, …, M. Prieto. 2012. The photophysics of a Rhodamine head labeled phospholipid in the identification and characterization of membrane lipid phases. *Chem. Phys. Lipids.* 165:311–319.

44. Jmoudiak, M., and A. H. Futerman. 2005. Gaucher disease: pathological mechanisms and modern management. *Br. J. Haematol.* 129:178–188.

45. Hazemoto, N., M. Harada, …, Y. Kato. 1993. Effect of phosphatidylcholine and cholesterol on pH-sensitive liposomes. *Chem. Pharm. Bull. (Tokyo).* 41:1003–1006.

46. Bailey, A. L., M. A. Monck, and P. R. Cullis. 1997. pH-induced destabilization of lipid bilayers by a lipopeptide derived from influenza hemagglutinin. *Biochim. Biophys. Acta.* 1324:232–244.

47. Dewick, P. M. 2006. Acids and bases. *In* Essentials of Organic Chemistry: For Students of Pharmacy, Medicinal Chemistry and Biological Chemistry. P. M. Dewick, editor. John Wiley & Sons, Hoboken, pp. 120–164.

48. Magarkar, A., V. Dhawan, …, A. Bunker. 2014. Cholesterol level affects surface charge of lipid membranes in saline solution. *Sci. Rep.* 4:5005.

49. Rhines, F. N. 1956. Phase diagrams in metallurgy: their development and application. McGraw-Hill.

50. Baker, H. 1992. ASM Handbook: Alloy Phase Diagrams. ASM International, Materials Park, OH.

51. Castro, B. M., R. F. M. de Almeida, …, M. Prieto. 2007. Formation of ceramide/sphingomyelin gel domains in the presence of an unsaturated phospholipid: a quantitative multiprobe approach. *Biophys. J.* 93:1639–1650.

52. Bates, D. M., and D. G. Watts. 2008. Nonlinear regression: iterative estimation and linear approximations. *In* Nonlinear Regression Analysis and Its Applications. John Wiley & Sons, pp. 32–66.

53. Sot, J., M. Ibarguren, …, A. Alonso. 2008. Cholesterol displacement by ceramide in sphingomyelin-containing liquid-ordered domains, and generation of gel regions in giant lipidic vesicles. *FEBS Lett.* 582:3230–3236.

54. Pinto, S. N., L. C. Silva, …, M. Prieto. 2011. Effect of ceramide structure on membrane biophysical properties: the role of acyl chain length and unsaturation. *Biochim. Biophys. Acta.* 1808:2753–2760.

55. Carrer, D. C., S. Härtel, …, B. Maggio. 2003. Ceramide modulates the lipid membrane organization at molecular and supramolecular levels. *Chem. Phys. Lipids.* 122:147–152.

56. Paroutis, P., N. Touret, and S. Grinstein. 2004. The pH of the secretory pathway: measurement, determinants, and regulation. *Physiology (Bethesda).* 19:207–215.

57. Riemann, A., A. Ihling, …, O. Thews. 2013. Impact of extracellular acidosis on intracellular ph control and cell signaling in tumor cells. *In* Oxygen Transport to Tissue XXXV. S. Van Huffel, G. Naulaers, A. Caicedo, D. F. Bruley, and D. K. Harrison, editors. Springer, New York, pp. 221–228.